

Chapter 20

Dynamics of a System of Two Coupled MEMS Oscillators



Richard H. Rand, Alan T. Zehnder, B. Shayak and Aditya Bhaskar

Abstract We investigate the dynamics of two limit cycle MEMS oscillators connected via spring coupling. Each individual oscillator is based on a MEMS structure which moves within a laser-driven interference pattern. As the structure vibrates, it changes the interference gap, causing the quantity of absorbed light to change, producing a feedback loop between the motion and the absorbed light and resulting in a limit cycle oscillation. A simplified model of this MEMS oscillator, omitting parametric feedback and structural damping, has been previously presented (Rand et al in Proceedings of 9th European Nonlinear Dynamics Conference (ENOC 2017), 2017, [3]). For the coupled system, a perturbation method is used to obtain a slow flow which is investigated using AUTO and numerical integration. Various bifurcations which occur as a result of changing the coupling strength are identified.

Keywords Coupled oscillators · MEMS · Bifurcations · Perturbations

20.1 Introduction

This work is motivated by a type of MEMS device in which a laser is used to determine the motion of the device by interference. The MEMS device is typically a clamped-clamped beam fabricated from a thin layer of Si and suspended above a Si substrate. Laser light is focused onto the beam surface and is partially reflected, absorbed and

R. H. Rand (✉) · A. T. Zehnder · B. Shayak · A. Bhaskar
Theoretical and Applied Mechanics, Sibley School of Mechanical and Aerospace Engineering,
and Department of Mathematics, Cornell University, Ithaca, NY 14853, USA
e-mail: rrh2@cornell.edu

A. T. Zehnder
e-mail: atz2@cornell.edu

B. Shayak
e-mail: sb2344@cornell.edu

A. Bhaskar
e-mail: ab2823@cornell.edu

transmitted. The transmitted portion is further reflected from the substrate and will interfere with the reflected light to form a cavity interferometer. The net effect is that both the reflected and absorbed light are periodic functions of the gap between the beam and the substrate. Thus, vibration of the beam will modulate both the reflected and absorbed light. The reflected light, directed to an AC coupled photo diode is used to transduce the motion of the MEMS device.

The absorbed portion of the laser light causes heating of the MEMS device by the laser beam, resulting in the deflection of the device, which then changes the amount of heat absorbed, with the net effect of feedback between the motion and the thermal heating, which can produce limit cycle (LC) oscillations.

We are interested in studying the dynamics of a system of such coupled LC oscillators. Each one consists of an elastic system, modeled as a second order ODE, coupled to a first order ODE representing the heat transfer due to the laser heating effects.

A system of this kind was studied by Aubin et al. in [1], and may be written in the following form:

$$\ddot{z} + \frac{\dot{z}}{Q} + (1 + CT)z + \beta z^3 = DT, \quad (20.1)$$

$$\dot{T} + BT = HP[a + \gamma \sin^2 2\pi(z - z_0)] \quad (20.2)$$

Here z is the displacement of a mechanical oscillator and T is its temperature due to laser illumination. In the mechanical equation Q is the quality factor, C is the stiffness change due to temperature, D is the displacement due to temperature and β is the coefficient of the cubic nonlinearity. In the thermal equation the quantities a and γ represent the average and contrast of the absorption of laser power, P is the laser power, H and B represent the thermal mass and heat loss rate. The offset, z_0 , models the equilibrium position of the oscillator with respect to the interference field created by the oscillator/gap/substrate stack. This complicated model, which includes effects of damping, stiffness change due to heating, periodic dependence of light absorption on interferometric gap, and nonlinearity, was shown to support LC oscillations.

In a recent paper, Zehnder et al. [2] considered a coupled system of two such LC oscillators:

$$\ddot{z}_1 + \frac{\dot{z}_1}{Q} + (1 + CT_1)z_1 + \beta z_1^3 + \frac{V^2(z_1 - z_2)}{1 + |z_1 - z_2|^p} = DT_1, \quad (20.3)$$

$$\dot{T}_1 + BT_1 = HP[a + \gamma \sin^2(2\pi(z_1 - z_0))], \quad (20.4)$$

$$\ddot{z}_2 + \frac{\dot{z}_2}{Q} + \kappa(1 + CT_2)z_2 + \beta z_2^3 + \frac{V^2(z_2 - z_1)}{1 + |z_2 - z_1|^p} = DT_2, \quad (20.5)$$

$$\dot{T}_2 + BT_2 = HP[a + \gamma \sin^2(2\pi(z_2 - z_0))]. \quad (20.6)$$

Here the V^2 terms represent electrostatic fringing field coupling, see Fig. 20.1.

Numerous interesting effects were observed in this numerical study of the governing differential equations, including regions of 1:1 locking, and more generally of $m:n$ locking. However, these differential equations are very complicated and it

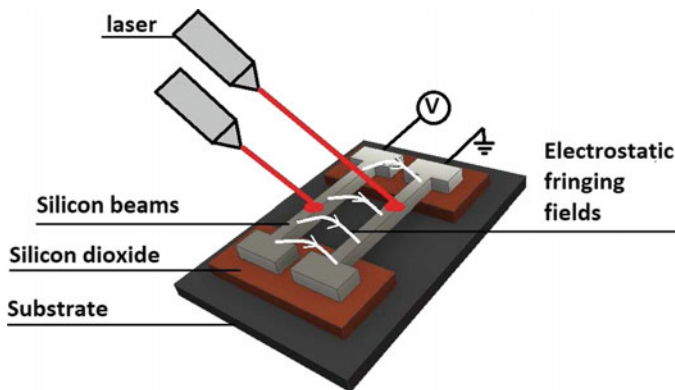


Fig. 20.1 A system of two coupled MEMS oscillators

is hard to tell which terms are responsible for the changes in qualitative dynamical behavior. Thus, in order to better understand the dynamics, we posited a simpler system which omitted effects such as damping, nonlinearity and stiffness changes due to heating [3]:

$$\ddot{z} + z = T \quad \text{and} \quad \dot{T} + T = z^2 - pz \quad (20.7)$$

To produce the simplest possible model, all constants have been taken equal to unity. The parameter z_0 in Eqs. (20.3)–(20.6) is referred to as p and takes on a representative value of 0.1. Numerical integration shows that this system supports a limit cycle [3].

In the present study, two oscillators of the form of Eq. (20.7) are considered, connected via spring coupling. The equations of motion are:

$$\ddot{z}_1 + z_1 = T_1 + \alpha(z_2 - z_1) \quad \text{and} \quad \dot{T}_1 + T_1 = z_1^2 - pz_1 \quad (20.8)$$

$$\ddot{z}_2 + z_2 = T_2 + \alpha(z_1 - z_2) \quad \text{and} \quad \dot{T}_2 + T_2 = z_2^2 - pz_2 \quad (20.9)$$

where α is a positive parameter, the coupling strength. The spring coupling is analogous to the electrostatic fringing field of Eqs. (20.3), (20.5), see Fig. 20.1.

20.2 Perturbations

In order to prepare Eqs. (20.8), (20.9) for treatment by perturbations, a parameter ε is introduced as follows:

$$\ddot{z}_1 + z_1 = \varepsilon T_1 + \varepsilon^2 \alpha(z_2 - z_1) \quad \text{and} \quad \dot{T}_1 + T_1 = z_1^2 - \varepsilon pz_1 \quad (20.10)$$

$$\ddot{z}_2 + z_2 = \varepsilon T_2 + \varepsilon^2 \alpha(z_1 - z_2) \quad \text{and} \quad \dot{T}_2 + T_2 = z_2^2 - \varepsilon pz_2 \quad (20.11)$$

We use a three variable perturbation method (also known as multiple scales) [4], which involves replacing the independent variable t with three new variables, $\xi = t$, $\eta = \varepsilon t$ (slow time) and $\zeta = \varepsilon^2 t$ (very slow time). The chain rule gives:

$$\frac{dz}{dt} = \frac{\partial z}{\partial \xi} \frac{d\xi}{dt} + \frac{\partial z}{\partial \eta} \frac{d\eta}{dt} + \frac{\partial z}{\partial \zeta} \frac{d\zeta}{dt} = \frac{\partial z}{\partial \xi} + \varepsilon \frac{\partial z}{\partial \eta} + \varepsilon^2 \frac{\partial z}{\partial \zeta} \tag{20.12}$$

$$\frac{d^2z}{dt^2} = \frac{\partial^2 z}{\partial \xi^2} + 2\varepsilon \frac{\partial^2 z}{\partial \eta \partial \xi} + \varepsilon^2 \left(\frac{\partial^2 z}{\partial \zeta \partial \xi} + \frac{\partial^2 z}{\partial \eta^2} \right) \tag{20.13}$$

Next all 4 variables z_1, T_1, z_2, T_2 are expanded in power series in ε and are substituted into Eqs. (20.10), (20.11). After collecting like powers of ε , we obtain:

$$z_1 = A(\zeta) \cos \xi + B(\zeta) \sin \xi + O(\varepsilon) \quad \text{and} \quad z_2 = C(\zeta) \cos \xi + D(\zeta) \sin \xi + O(\varepsilon) \tag{20.14}$$

where the slowly varying parameters A, B, C, D are determined by the following slow flow, which is obtained by eliminating secular terms from the $O(\varepsilon^2)$ equations:

$$\frac{dA}{d\zeta} = -\frac{60\alpha D + 31B^3 + 27AB^2 + (31A^2 - 30p - 60\alpha)B + 27A^3 - 30pA}{120} \tag{20.15}$$

$$\frac{dB}{d\zeta} = \frac{60\alpha C - 27B^3 + 31AB^2 + (30p - 27A^2)B + 31A^3 + (-30p - 60\alpha)A}{120} \tag{20.16}$$

$$\frac{dC}{d\zeta} = -\frac{31D^3 + 27CD^2 + (31C^2 - 30p - 60\alpha)D + 27C^3 - 30pC + 60\alpha B}{120} \tag{20.17}$$

$$\frac{dD}{d\zeta} = -\frac{27D^3 - 31CD^2 + (27C^2 - 30p)D - 31C^3 + (30p + 60\alpha)C - 60\alpha A}{120} \tag{20.18}$$

These equations can be simplified by transforming to polar coordinates:

$$A = r_1 \cos \theta_1, \quad B = r_1 \sin \theta_1, \quad C = r_2 \cos \theta_2, \quad D = r_2 \sin \theta_2, \tag{20.19}$$

with the following result, where $\varphi = \theta_2 - \theta_1$:

$$\frac{dr_1}{d\zeta} = \frac{pr_1}{4} - \frac{9r_1^3}{40} - \frac{\alpha}{2} r_2 \sin \varphi \tag{20.20}$$

$$\frac{dr_2}{d\zeta} = \frac{pr_2}{4} - \frac{9r_2^3}{40} + \frac{\alpha}{2} r_1 \sin \varphi \tag{20.21}$$

$$\frac{d\varphi}{d\zeta} = \frac{31}{120} (r_2^2 - r_1^2) + \frac{\alpha}{2} \cos \varphi \left(\frac{r_1}{r_2} - \frac{r_2}{r_1} \right) \tag{20.22}$$

The rest of this paper is based on an analysis of these last three equations.

20.3 Bifurcations

The first thing to notice about Eqs. (20.20)–(20.22) is that they exhibit a symmetry: they are invariant under the transformation

$$r_1 \longrightarrow r_2, \quad r_2 \longrightarrow r_1, \quad \varphi \longrightarrow -\varphi \tag{20.23}$$

As we will see, this symmetry will have a profound effect on the bifurcations associated with Eqs. (20.20)–(20.22).

Let us begin by looking for equilibria in the slow flow (20.20)–(20.22). These turn out to satisfy

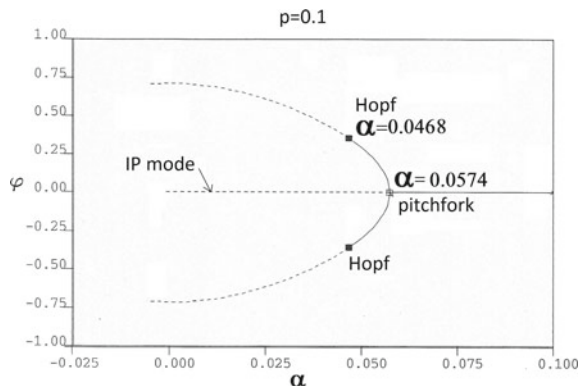
$$r_1 = r_2 = \frac{\sqrt{10p}}{3} \quad \text{and} \quad \sin \varphi = 0 \implies \varphi = 0 \text{ or } \pi \tag{20.24}$$

Here $\varphi = 0$ corresponds to the in phase (IP) mode and $\varphi = \pi$ corresponds to the out of phase (OP) mode.

As a first step in understanding the bifurcations occurring in Eqs. (20.20)–(20.22), we use the bifurcation software AUTO [5]. See Fig. 20.2 where equilibrium points in the slow flow are displayed using the convention that a solid (dashed) line represents a stable (unstable) equilibrium. Limit cycles in the slow flow (born in a Hopf bifurcation) are not shown. The OP mode at $\varphi = \pi$ is not shown, and is stable.

Note that for $\alpha > 0.0574$ AUTO predicts that both the IP and OP modes are stable. These slow flow equilibria are separated by an unstable slow flow limit cycle which we shall refer to as a separatrix. Moving from the 3 dimensional slow flow space to the 6 dimensional space of Eqs. (20.8), (20.9), the separatrix appears as a quasiperiodic motion. Although it is unstable we may nevertheless see what the separatrix looks like by numerically integrating Eqs. (20.8), (20.9) for initial conditions of the form $(z_1(0), \dot{z}_1(0), T_1(0), z_2(0), \dot{z}_2(0), T_2(0)) = (0.1, 0, 0, \mu, 0, 0)$, and iteratively varying μ so that the large time behavior (approximately) lies on the basin boundary between the two equilibria. See Fig. 20.3 where we find that $\mu \approx 0.0021$ for $\alpha = 0.07$.

Fig. 20.2 AUTO bifurcation diagram for Eqs. (20.20)–(20.22). A solid (dashed) line represents a stable (unstable) equilibrium point in the slow flow. Limit cycles in the slow flow born in the Hopf bifurcations are not shown. The OP mode at $\varphi = \pi$ is not shown, and is stable



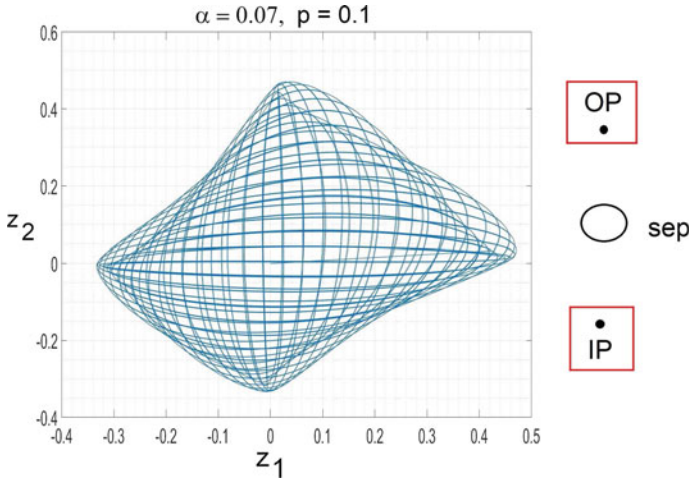


Fig. 20.3 LEFT: Separatrix motion, unstable, separates stable IP and OP modes. RIGHT: Schematic view showing IP, OP and separatrix. Stable motions are boxed in Red

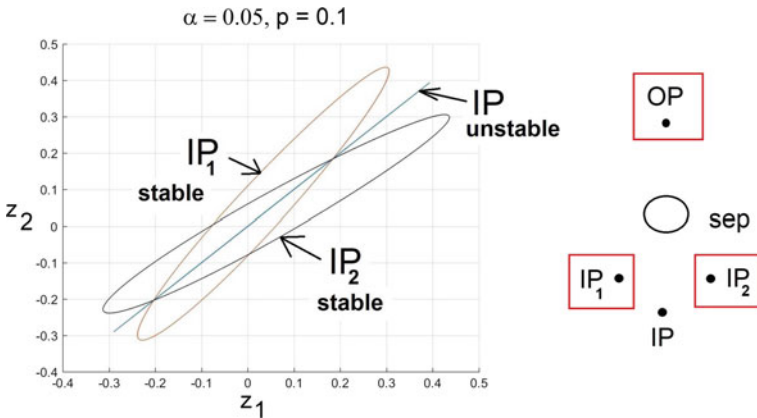


Fig. 20.4 LEFT: Two new slow flow equilibria are born in a pitchfork, denoted by IP_1 and IP_2 . In the 6 dimensional space these are seen to be periodic motions, symmetrically located about the IP mode. RIGHT: Schematic view showing IP_1 , IP_2 , IP, OP and separatrix. Stable motions are boxed in Red

From Fig. 20.2 we see that when α is decreased through 0.0574, the IP mode loses stability in a pitchfork bifurcation. Two new slow flow equilibria are born in this pitchfork, denoted by IP_1 and IP_2 . In the 6 dimensional space these are seen to be periodic motions, see Fig. 20.4.

From Fig. 20.2 we see that when α is further decreased through 0.0468, the slow flow equilibria IP_1 and IP_2 lose stability in Hopf bifurcations, resulting in stable slow flow limit cycles LC_1 and LC_2 . In the 6 dimensional space these are seen to be quasiperiodic motions, see Fig. 20.5.

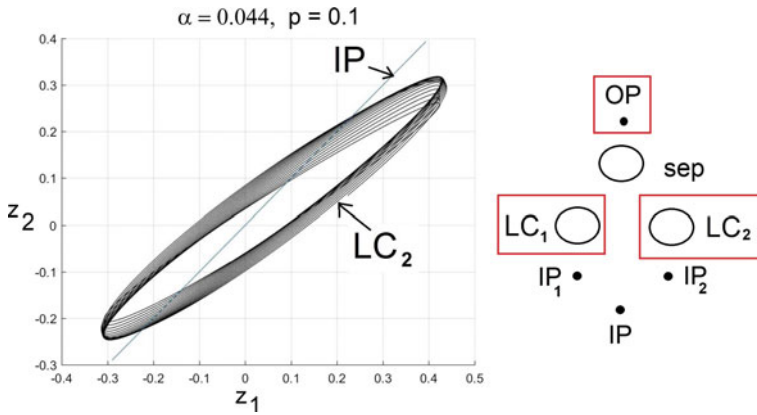


Fig. 20.5 LEFT: Two new slow flow limit cycles are born in Hopf bifurcations, denoted by LC_1 and LC_2 . In the 6 dimensional space these are seen to be quasiperiodic motions, symmetrically located about the IP mode, cf. Fig. 20.4. Note: For clarity of presentation, LC_1 is not shown. RIGHT: Schematic view showing LC_1 , LC_2 , IP_1 , IP_2 , IP, OP and separatrix. Stable motions are boxed in Red

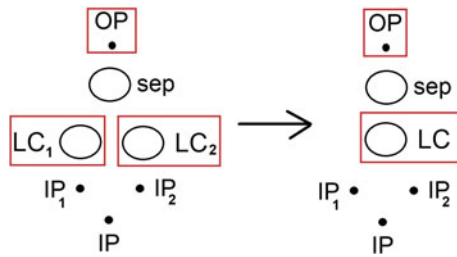


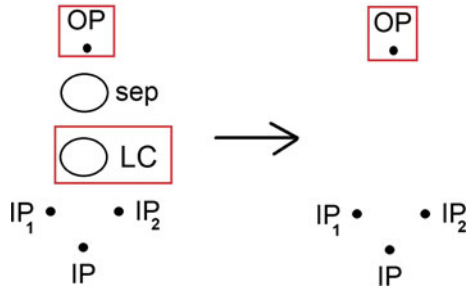
Fig. 20.6 A schematic representation of the double homoclinic bifurcation in which the asymmetric slow flow limit cycles LC_1 and LC_2 join to become a single slow flow limit cycle LC which exhibits the symmetry of Eq. (20.23). Stable motions are boxed in Red

A further bifurcation occurs when α decreases through approximately 0.0436, though this is not shown in Fig. 20.2. In this case there is a homoclinic bifurcation in which the asymmetric slow flow limit cycles LC_1 and LC_2 join to become a single slow flow limit cycle LC which exhibits the symmetry of Eq. (20.23). See Fig. 20.6.

Another bifurcation occurs when α decreases through approximately 0.0415, in which two slow flow limit cycles merge together in a limit cycle fold and disappear. Specifically, the unstable separatrix limit cycle “sep” merges simultaneously and symmetrically with the symmetric slow flow stable limit cycle “LC”. See Fig. 20.7. For values of α less than approximately 0.0415, the OP mode is the only stable motion.

The last two bifurcations (shown in Figs. 20.5 and 20.6) involve the merging of two limit cycles into a single limit cycle (a double homoclinic bifurcation), which is then followed by a limit cycle fold in which a stable and an unstable limit cycle come together and disappear. This sequence of bifurcations has been seen in other, unrelated dynamical systems. See [6] p. 376, Fig. 7.3.9, and [7] p. 69, Fig. 7.

Fig. 20.7 A schematic representation of the limit cycle fold in which two slow flow limit cycles merge together and disappear, leaving the OP mode as the only stable motion. Stable motions are boxed in Red



20.4 Conclusions

In this work we have investigated the dynamics of a system inspired by a pair of coupled identical MEMS oscillators, Eqs. (20.8), (20.9). Our method involved introducing a small parameter ϵ which permitted us to use a perturbation method, resulting in a slow flow, Eqs. (20.20)–(20.22). We then used AUTO and numerical integration to determine the various bifurcations which occurred when the coupling constant α was varied (for fixed parameter $p = 0.1$). Since the perturbation method is by its very nature approximate, we should not be surprised to find that the derived results are in some cases incorrect. In particular analysis of the slow flow predicts that both the IP and OP modes are stable for α sufficiently large. While this is true of the IP mode, linear stability analysis of the OP mode shows that it becomes unstable for $\alpha > 0.82$. Proof of this statement will be the subject of another paper by the same authors.

We noted that the derived slow flow (20.20)–(20.22) possessed a symmetry which led to nongeneric bifurcations such as a pitchfork and a homoclinic bifurcation with symmetry. A useful extension of this work will involve a comparable study of the dynamics of a pair of coupled nonidentical third order oscillators, which is not expected to display these kinds of nongeneric bifurcations.

Perhaps the most important lesson learned from this study is that the IP mode can be made stable by increasing the coupling between the oscillators. This result is reminiscent of a comparable property of similarly coupled van der Pol oscillators [4].

Acknowledgements The authors wish to thank Professor J. Guckenheimer for advising them on the bifurcations involved in this paper. This material is based upon work supported by the National Science Foundation under grant number CMMI-1634664.

References

1. Aubin, K., Zhalutdinov, M., Alan, T., Reichenbach, R.B., Rand, R., Zehnder, A., Parpia, J., Craighead, H.: Limit cycle oscillations in CW laser-driven NEMS. *J. Microelectromechanical Syst.* **13**, 1018–1026 (2004)
2. Zehnder, A.T., Rand, R.H., Krylov, S.: Phase locking of electrostatically coupled thermo-optically driven MEMS limit cycle oscillators. *Int. J. Non-Linear Mech.* **102**, 92–100 (2018)

3. Rand, R.H., Zehnder, A.T., Shayak B.: Analysis of a simplified MEMS oscillator. In: Proceedings of 9th European Nonlinear Dynamics Conference (ENOC 2017), 25–30 June 2017, Budapest, Hungary. <https://congressline.hu/enoc2017/abstracts/77.pdf> (2017)
4. Rand, R.H.: Lecture Notes in Nonlinear Vibrations. The Internet-First University Press. <http://ecommons.library.cornell.edu/handle/1813/28989> (2012)
5. Doedel, E.: see AUTO homepage. <http://indy.cs.concordia.ca/auto/> (1996)
6. Guckenheimer, J., Holmes, P.: Nonlinear Oscillations, Dynamical Systems, and Bifurcation of Vector Fields. Springer, Berlin (1983)
7. Lazarus, L., Davidow, M., Rand, R.: Dynamics of an oscillator with delay parametric excitation. *Int. J. Non-Linear Mech.* **78**, 66–71 (2016)